# Vibrational Analysis of 1,3,3-Trinitroazetidine Using Matrix Isolation Infrared Spectroscopy and Quantum Chemical Calculations

**Craig A. Thompson,† Jane K. Rice, and T. P. Russell***

*U.S. Naval Research Laboratory, Chemistry Division, Code 6110, Washington D.C. 20375-5342*

**Jorge M. Seminario and Peter Politzer**

*Department of Chemistry, University of New Orleans, New Orleans, Louisiana 70148*

*Received: April 3, 1997*[⊗]

Infrared spectra of 1,3,3-trinitroazetidine (TNAZ), $(O_2N)_2-C(CH)_2N-NO_2$, were obtained for samples evaporated from a Knudsen Cell and codeposited with argon on a 15 K IR window. Spectra of matrix-isolated TNAZ and isotopically labeled TNAZ are used to assign 24 of the 45 fundamental molecular vibrations. Comparisons among experimental spectra and spectra calculated using Hartree−Fock (HF), second-order Moller-Plesset theory (MP2) and three density functional theory (DFT) methods indicate that DFT gives a more accurate vibrational description than MP2 or HF. The DFT approach was further explored using the BP86 and the hybrid B3P86 and B3LYP methods. Overall best results were obtained with BP86 and B3LYP.

## Introduction

There is currently a great deal of interest in characterizing 1,3,3-trinitroazetidine (TNAZ) and understanding its decomposition chemistry.[1−4] TNAZ, now recognized as an important additive in fuels and propellant formulations, was first synthesized in the late 1980s.[5] Its low melting point (101 °C) and thermal stability to 240 °C render it steam castable. However, only recently have economic synthetic routes for affordable large-scale production been developed. Chemically, TNAZ is of interest for many reasons. It contains a four-member ring, shown in Figure 1, with 37 kcal/mol strain energy.[3] Due in part to this strain energy, TNAZ is at least 10% more energetic than the most powerful explosives currently in use.[4] There is also interest in the chemistry of cyclic nitramines containing *gem*-dinitro groups; TNAZ is the simplest molecule in this class.[5]

Molecular spectroscopic studies of TNAZ include IR spectra of TNAZ in solution,[6] as a dispersed powder in KBr pellets,[7] and as thin solid films.[8] The solution and solid phase spectra are characterized by intermolecular interactions that result in broad bands that complicate the vibrational analysis. Therefore, matrix isolation techniques in combination with infrared spectroscopy were employed in this study to identify and assign the fundamental molecular vibrations.

X-ray crystallography indicates the *gem*-dinitro groups of crystalline TNAZ are oriented with their bond planes perpendicular to each other.[5] Infrared studies of decomposition reactions induced by multiphoton dissociation of TNAZ have yielded information about decomposition pathways,[9] as have mass spectroscopic and infrared studies of thermal decomposition.[10,11] In addition, $^1H$ and $^{13}C$ NMR studies have provided structural information.[6] Solution phase IR spectra of TNAZ in methylene chloride reveal CH stretching modes at 3050 $cm^{-1}$ and $NO_2$ modes at 1580 and 1420 $cm^{-1}$.[6] To our knowledge, no studies of gas phase vibrational levels of TNAZ have been reported.

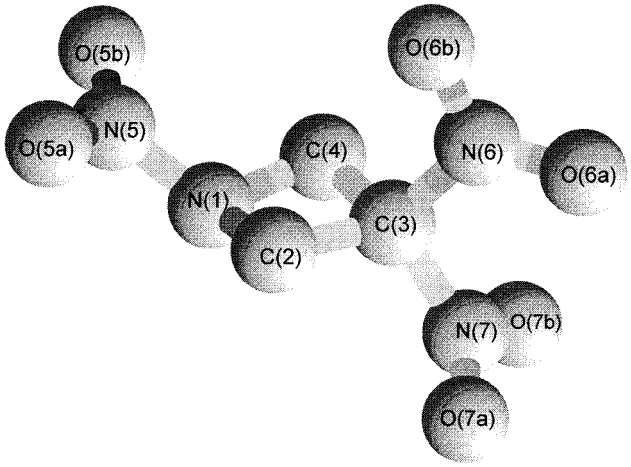


**Figure 1.** Structure of 1,3,3-trinitroazetidine including the numbering scheme for atoms in Table 3 (hydrogen atoms not shown).

Recently, the application of quantum mechanical calculations to energetic materials has expanded. These calculations provide predictions of molecular parameters including bond lengths and frequencies of fundamental molecular vibrations. In addition, quantum mechanical studies provide insight into reaction pathways either by calculating the thermodynamics associated with bond cleavage or by examining the energetics along an internal reaction coordinate.[12,13] In the past correlated *ab initio* quantum mechanical studies for systems as large as TNAZ have been limited by computing power. Recently, density functional theory (DFT) has emerged as a useful method for quantum chemical studies since it is computationally less intensive and does include electron correlation effects.[14,15] However, the availability of several correlation and exchange functionals suggests a need for comparison of the effectiveness of various options.

Accurate experimental assignment of the molecular vibrations permits a systematic study of the accuracy of the force field calculations using a variety of quantum chemical methods. Recently, computational studies of several ring systems such as thiophene and furan[16] and large ring systems[17] have provided interesting results but do not provide guidelines as to the preferred approach for highly strained ring systems, such as

* Author to whom correspondence should be addressed.
† Naval Research Laboratory/National Research Council Associate.
⊗ Abstract published in *Advance ACS Abstracts,* August 1, 1997.

S1089-5639(97)01173-0 

TNAZ. In this work, the calculated and observed fundamental molecular vibrations of TNAZ are compared. Specifically, infrared spectra for matrix-isolated TNAZ are compared to calculated results using Hartree−Fock (HF), post-Hartree−Fock, and DFT methods.

## Experimental Section

**Materials.** Samples of TNAZ obtained from Thiokol Inc. were used as received. Samples of isotopically labeled TNAZ, $(O_2N)_2-C(CH_2)_2N-{}^{15}NO_2$, $(O_2{}^{15}N)_2-C(CH_2)_2N-{}^{15}NO_2$, and $(O_2N)_2-{}^{13}C(CH_2)_2N-NO_2$ were synthesized by M. Coburn and were as received.[18]

**Matrix Isolation.** Matrix-isolated samples of TNAZ were prepared in a vacuum chamber maintained at a background pressure of $\sim 1 \times 10^{-7}$ Torr. TNAZ was thermally evaporated from a resistively heated Knudsen cell at temperatures ranging from 55 to 75 °C. Temperature was maintained using an Omega 76133 temperature controller. A 250 $\mu$m orifice was required for the cap of the Knudsen cell due to the relatively high vapor pressure of TNAZ. An argon gas spray (MG Industries, 99.999%) adjacent to the Knudsen cell was used to transport and deposit the sample on the cold window.

Matrix samples were collected on a CsI salt window maintained at 15 K by an Air Products, DE-202, closed-cycle helium refrigerator. Deposition times ranged from 2 to 3 h at a Knudsen cell temperature of 65 °C. Under these conditions, the optimal argon flow rate was 2 mmol/h. TNAZ deposition rates were approximately 10 $\mu$mol/h, providing a mole ratio of TNAZ:Ar ~1:200. Once formed, samples were analyzed using a Nicolet 740 spectrometer with a mercury-cadmium-telluride (MCT-A) detector. For each sample, 256 spectra were averaged yielding a spectrum with 0.1 $cm^{-1}$ accuracy and 0.5 $cm^{-1}$ resolution.

**Quantum Chemical Calculations.** Quantum chemical calculations were carried out using the commercially available suite of programs, Gaussian 94 D.[19] Studies were done using a Cray C90 supercomputer at the Army Corp of Engineers Waterways Experiment Station Center for High Performance Computing. The computer employed 16 processors that provided a peak speed of 16 Gflops. Hartree−Fock calculations were conducted for comparison with second-order Moller−Plesset (MP2) results. MP2 is the simplest and least expensive available correlated method. The basis set for all calculations including DFT was 6-31G** for all atoms.

Two exchange and two correlation functionals were employed in comparing DFT results to HF and MP2. First, Becke's 88 exchange[20] was used with Perdew's 86 correlation functional[21,22] (BP86). Next, Becke's three-parameter hybrid method[23] was combined with Perdew's 86 correlation functional (B3P86) to permit comparisons to the BP86 method. Finally, Becke's three-parameter hybrid was used with the Lee−Yang−Parr correlation functional[24] (B3LYP).

Calculations of optimized geometry were initiated in both $C_1$ and $C_s$ symmetries to confirm the relative equilibrium orientations of the $NO_2$ groups. In all cases, the optimized structure was consistent with the $C_s$ structure shown in Figure 1. Frequency calculations were accordingly performed in $C_s$ symmetry.

Harmonic frequencies for TNAZ using HF, MP2, BP86, B3P86, and B3LYP were calculated for force fields obtained analytically from the sets of second derivatives of the energy. Frequencies for isotopically labeled TNAZ were recalculated following mass substitution using the force constants obtained for the most common isotope.

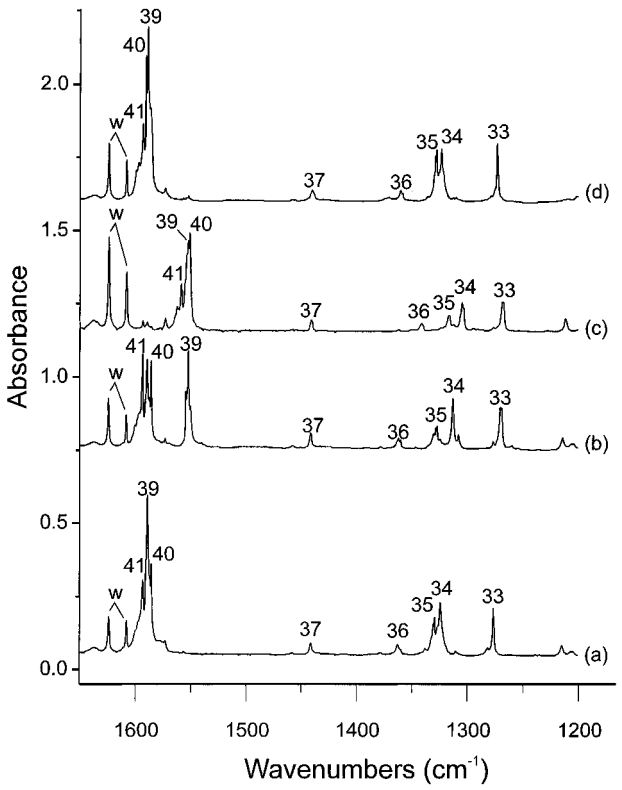


**Figure 2.** Experimental spectra for 1,3,3-trinitroazetidine (TNAZ) and isotopically labeled TNAZ from 1900 to 1200 $cm^{-1}$: (a) TNAZ in solid Ar at 15 K; (b) $(O_2N)_2-C(CH_2)_2N-{}^{15}NO_2$ in solid Ar at 15 K; (c) $(O_2{}^{15}N)_2-C(CH_2)_2N-{}^{15}NO_2$ in solid Ar at 15 K; (d) $(O_2N)_2-{}^{13}C(CH_2)_2N-NO_2$ in solid Ar at 15 K.

## Results

**Experimental Spectra.** Experimental spectra for matrix-isolated samples of TNAZ and isotopically labeled TNAZ are presented first, followed by results of quantum chemical calculations. The spectra of matrix-isolated TNAZ are characterized by intense and sharp vibrational bands. The observed IR features (Figures 2−6) have their corresponding mode number assignments labeled. These assignments are made from comparisons of all experimental spectra and the quantum mechanical calculations. TNAZ has 45 fundamental vibrations; several are not expected to be detected because they are either too weak or appear below the limit of detection (600 $cm^{-1}$) in this study.

Assignments for the experimental IR absorption frequencies for TNAZ are listed in Table 1. Figure 2a shows the normal abundance TNAZ spectrum from 1650 to 1200 $cm^{-1}$. Three bands at 1593.2 (41), 1589.2 (39), and 1585.6 $cm^{-1}$ (40) are observed in the region expected for $NO_2$ antisymmetric stretching. Of these three absorptions, the middle (39) is unique in that it is most intense; it has two weak side bands at 1590.9 and 1587.1 $cm^{-1}$, which we attribute to matrix site splittings. Weaker absorptions at 1458.7 (38) and 1441.5 $cm^{-1}$ (37) are detected in the region expected for $CH_2$ bending modes. A group of absorptions (36−31) are observed in the regions expected for symmetric $NO_2$, N−N, and NC stretches. A relatively weak band at 1362.8 (36) is accompanied by two adjacent bands at 1329.5 (35) and 1324.5 $cm^{-1}$ (34) and a sharp band at 1276.7 $cm^{-1}$ (33). Three weak bands at 3027.3 (45), 2979.4 (44), and 2907.4 $cm^{-1}$ (43) appear in the region expected for CH stretches. In addition, two absorptions at 1623.8 and 1607.9 $cm^{-1}$ are in agreement with the Q and R branches of isolated water and are accordingly marked w.

**TABLE 1: Assignments for the Experimentally Observed Transitions ($cm^{-1}$) for TNAZ and Isotopically Labeled TNAZ**

| mode number | principal motion(s) | TNAZ $(O_2N)_2-C(CH_2)_2N-NO_2$ | $(O_2N)_2-C(CH_2)_2N-{}^{15}NO_2$ | $(O_2{}^{15}N)_2-C(CH_2)_2N-{}^{15}NO_2$ | $(O_2N)_2-{}^{13}C(CH_2)_2N-NO_2$ |
|---|---|---|---|---|---|
| 45 | $\nu_{as}(CH_2)$ | 3028.3 | 3028.7 | 3027.5 | 3027.6 |
| 44 | $\nu_{as}(CH_2)$ | 2979.4 | 2980.2 | 2979.3 | 2980.3 |
| 43 | $\nu_{s}(CH_2)$ | 2907.4 | 2907.8 | 2909.5 | 2907.2 |
| 41 | $\nu_{as}C-(NO_2)$ | 1593.2 | 1593.5 | 1558.9 | 1589.1 |
| 40 | $\nu_{as}N-(NO_2)$ | 1585.6 | 1585.9 | 1551.3 | 1593.4 |
| 39 | $\nu_{as}C-(NO_2)$ | 1589.2 | 1552.6 | 1552.7 | 1590.7 |
| 38 | $\delta(CH_2)$ | 1458.7 | 1457.0 | 1457.9 | 1457.9 |
| 37 | $\delta(CH_2)$ | 1441.5 | 1441.5 | 1441.5 | 1440.6 |
| 36 | $\delta CH_2/\nu_{as}(NCN)$ | 1362.8 | 1362.1 | 1341.4 | 1360.6 |
| 35 | $\sigma(NN)/\delta(CH_2)/\nu_{as}(NCN)$ | 1329.5 | 1327.4 | 1317.1 | 1328.0 |
| 34 | $\sigma(NN)/\nu_{as}(NCN)/\nu_{s}(NO_2)$ | 1324.5 | 1313.0 | 1304.9 | 1323.8 |
| 33 | ring/$CH_2$ | 1276.7 | 1270.0 | 1268.2 | 1273.8 |
| 31 | ring/$CH_2$ | 1215.3 | 1214.7 | 1212.3 | 1192.0 |
| 30 | ring/$CH_2$ | 1207.3 | 1206.7 | 1199.5 | 1202.4 |
| 29 | ring/$CH_2$ | 1158.7 | 1158.6 | 1157.7 | 1146.5 |
| 28 | ring/$CH_2$ | 1123.0 | | 1130.0 | 1116.2 |
| 26 | ring/$CH_2$ | 1091.1 | 1091.1 | 1090.1 | 1069.9 |
| 25 | ring/$CH_2$ | 1039.9 | 1038.7 | 1037.4 | 1029.7 |
| 23 | ring/$CH_2$ | 905.8 | 903.9 | 902.6 | 904.2 |
| 22 | NN/ring/$CH_2$ | 864.8 | 864.8 | 860.6 | 865.5 |
| 21 | ring/$CH_2$ | 840.9 | 840.4 | 833.1 | 840.3 |
| 20 | $\delta N-(NO_2)/CH_2$ | 817.2 | 811.1 | 809.7 | 817.0 |
| 19 | $\delta N-(NO_2)/CH_2$ | 766.2 | 750.5 | 749.7 | 766.7 |
| 16 | ring/$\delta C-(NO_2)/CH_2$ | 658.5 | 658.4 | | |

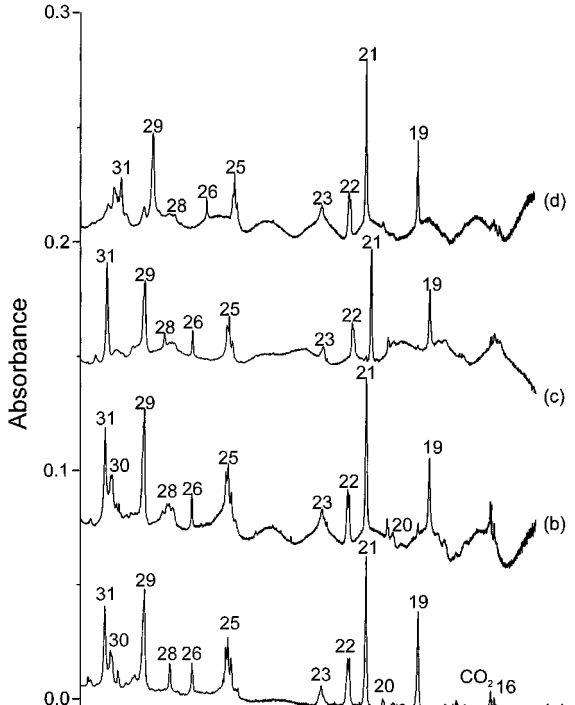


**Figure 3.** Experimental spectra for 1,3,3-trinitroazetidine (TNAZ) and isotopically labeled TNAZ from 1250 to 600 $cm^{-1}$: (a) TNAZ in solid Ar at 15 K; (b) $(O_2N)_2-C(CH_2)_2N-{}^{15}NO_2$ in solid Ar at 15 K; (c) $(O_2{}^{15}N)_2-C(CH_2)_2N-{}^{15}NO_2$ in solid Ar at 15 K; (d) $(O_2N)_2-{}^{13}C-(CH_2)_2N-NO_2$ in solid Ar at 15 K.

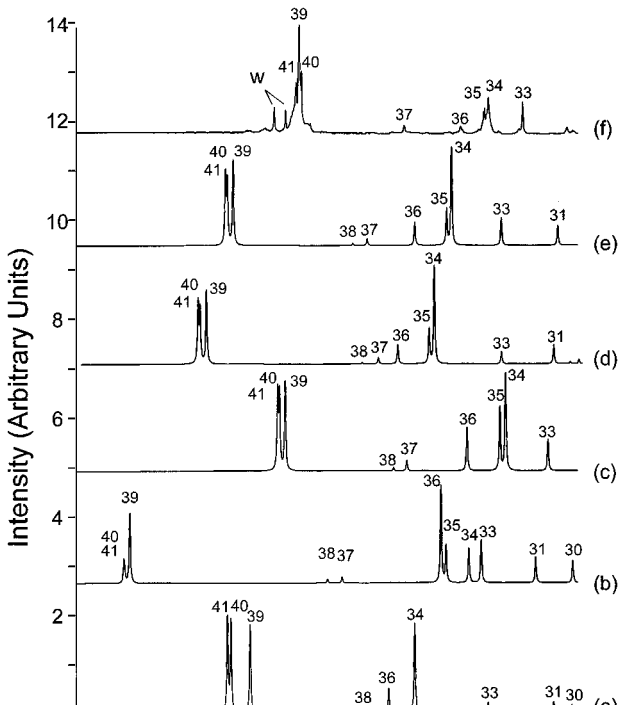


**Figure 4.** Comparison of calculated and observed spectra for 1,3,3-trinitroazetidine from 1900 to 1200 $cm^{-1}$: (a) calculated with scaled (0.89) HF/6-31G**; (b) calculated with unscaled MP2/6-31G**; (c) calculated with unscaled BP86/6-31G**; (d) calculated with unscaled B3P86/6-31G**; (e) calculated with unscaled B3LYP/6-31G**; (f) matrix-isolated TNAZ in solid Ar at 15 K.

The TNAZ spectrum from 1200 to 600 $cm^{-1}$ is shown in Figure 3a. Absorptions below 1200 $cm^{-1}$ are expected to belong to ring modes and $NO_2$ bending and wagging modes. A sharp absorption at 1215.3 $cm^{-1}$ (31) is accompanied by a weaker one at 1207.3 $cm^{-1}$ (30). A sharp absorption at 1158.7 $cm^{-1}$ (29) is accompanied by two medium intensity ones at 1123.0 (28) and 1091.1 $cm^{-1}$ (26). A triplet of bands at 1042.8, 1039.6, and 1035.3 $cm^{-1}$ is attributed to matrix site splitting of a single vibrational mode (25).

Six features are observed below 1000 $cm^{-1}$. A broad absorption at 905.8 $cm^{-1}$ (23) is accompanied by a doublet at 867.2 and 864.8 $cm^{-1}$ (22). The most intense absorption of the lower energy region at 840.9 $cm^{-1}$ (21) is accompanied by a weak absorption at 817.2 $cm^{-1}$ (20) and a band at 766.2 $cm^{-1}$

**TABLE 2: Comparing Calculated and Observed Geometry Parameters (angstroms and degrees) for 1,3,3-Trinitroazetidine**

| parameter | X-ray[a] | HF | MP2 | BP86 | B3P86 | B3LYP |
|---|---|---|---|---|---|---|
| N(5)−N(1) | 1.351(6) | 1.3540 | 1.4051 | 1.4197 | 1.3863 | 1.3975 |
| C(3)−N(7) | 1.493(7) | 1.4912 | 1.4924 | 1.5260 | 1.5038 | 1.5137 |
| C(3)−N(6) | 1.517(7) | 1.4913 | 1.5051 | 1.5412 | 1.5119 | 1.5231 |
| N(5)−O(5b) | 1.236(5) | 1.1903 | 1.2349 | 1.2366 | 1.2191 | 1.2246 |
| N(5)−O(5a) | 1.218(5) | 1.1903 | 1.2349 | 1.2366 | 1.2191 | 1.2246 |
| N(7)−O(7b) | 1.212(6) | 1.1867 | 1.2402 | 1.2356 | 1.2167 | 1.2225 |
| N(7)−O(7a) | 1.217(6) | 1.1867 | 1.2402 | 1.2356 | 1.2167 | 1.2225 |
| N(6)−O(6a) | 1.214(5) | 1.1827 | 1.2384 | 1.2307 | 1.2131 | 1.2187 |
| N(6)−O(6b) | 1.223(6) | 1.1908 | 1.2382 | 1.2363 | 1.2182 | 1.2241 |
| N(1)−C(2) | 1.485(7) | 1.4626 | 1.4821 | 1.4901 | 1.4719 | 1.4811 |
| C(2)−C(3) | 1.534(7) | 1.5389 | 1.5331 | 1.5458 | 1.5350 | 1.5423 |
| N(1)−C(4) | 1.474(6) | 1.4626 | 1.4821 | 1.4901 | 1.4719 | 1.4811 |
| C(3)−C(4) | 1.545(7) | 1.5389 | 1.5331 | 1.5458 | 1.5350 | 1.5423 |
| C(2)−H(2a) | | 1.0766 | 1.0855 | 1.0991 | 1.0896 | 1.0895 |
| C(4)−H(4a) | | 1.0766 | 1.0855 | 1.0991 | 1.0896 | 1.0895 |
| C(2)−H(2b) | | 1.0798 | 1.0901 | 1.1019 | 1.0926 | 1.0920 |
| C(4)−H(4b) | | 1.0798 | 1.0901 | 1.1019 | 1.0926 | 1.0920 |
| ∠N(7)C(3)N(6) | 105.6(4) | 107.4 | 107.3 | 107.1 | 107.3 | 107.2 |
| ∠O(5b)N(5)O(5a) | 125.3(4) | 127.5 | 128.5 | 128.7 | 128.2 | 128.2 |
| ∠O(7b)N(7)O(7a) | 126.5(5) | 127.2 | 127.2 | 127.5 | 127.5 | 127.3 |
| ∠O(6a)N(6)O(6b) | 125.9(5) | 127.1 | 127.3 | 127.6 | 127.5 | 127.3 |
| ∠N(5)N(1)C(2) | 120.4(4) | 120.4 | 116.4 | 117.5 | 118.4 | 118.4 |
| ∠N(1)C(2)C(3) | 86.6(4) | 87.1 | 87.1 | 87.7 | 87.6 | 87.7 |
| ∠C(2)N(1)C(4) | 95.1(4) | 94.9 | 93.0 | 93.7 | 94.1 | 94.0 |
| ∠C(2)C(3)C(4) | 90.3(4) | 88.9 | 89.1 | 89.4 | 89.1 | 89.2 |
| ∠H(2a)C(2)H(2b) | | 111.5 | 111.8 | 111.2 | 111.3 | 111.2 |
| ∠H(4b)C(4)H(4a) | | 111.5 | 111.8 | 111.2 | 111.3 | 111.2 |

[a] Reference 5.

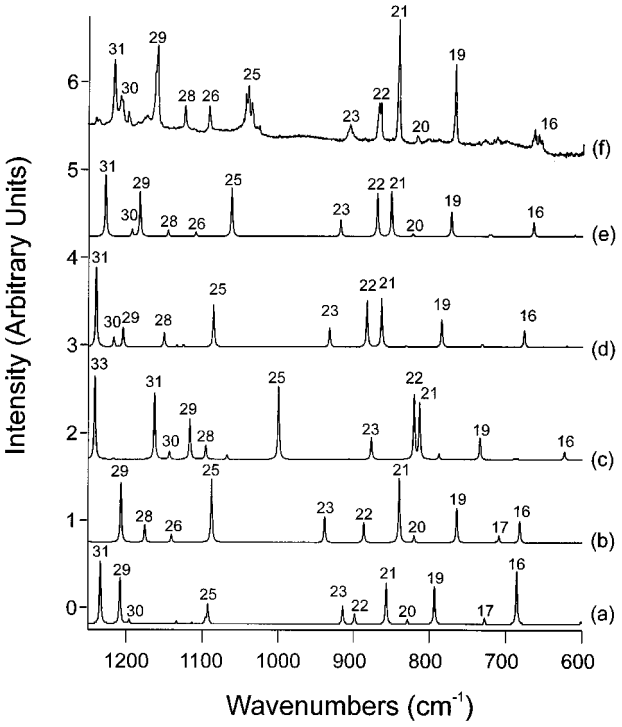


**Figure 5.** Comparison of calculated and observed spectra for 1,3,3-trinitroazetidine from 1250 to 600 $cm^{-1}$: (a) calculated with scaled (0.89) HF/6-31G**; (b) calculated with unscaled MP2/6-31G**; (c) calculated with unscaled BP86/6-31G**; (d) calculated with unscaled B3P86/6-31G**; (e) calculated with unscaled B3LYP/6-31G**; (f) matrix isolated TNAZ in solid Ar at 15 K.

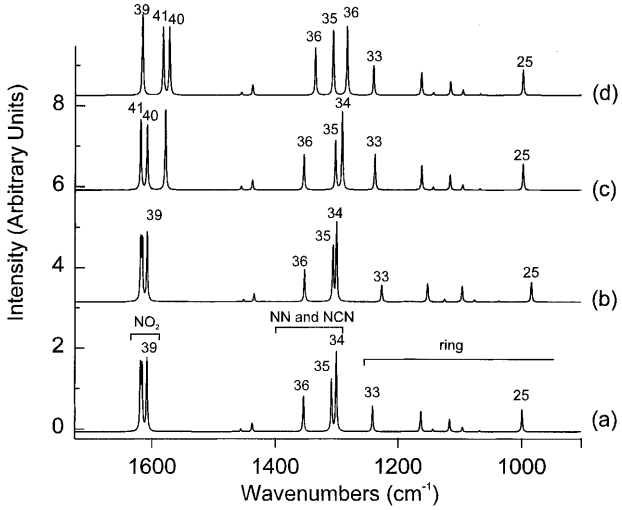


**Figure 6.** DFT calculated spectra for 1,3,3-trinitroazetidine using BP86/6-31G**: (a) most abundant isotope of TNAZ; (b) $(O_2N)-{}^{13}C-({}^{13}CH_2)_2N-NO_2$; (c) $(O_2N)_2-C(CH_2)_2N-{}^{15}NO_2$; (d) $(O_2{}^{15}N)_2-C(CH_2)_2-N-NO_2$.

(19). Finally, a weak $CO_2$ absorption at 663.6 $cm^{-1}$ is accompanied by a weak TNAZ feature at 658.5 $cm^{-1}$ (16).

Comparisons among spectra for TNAZ and isotopically labeled TNAZ are important for identifying participation of specific atoms in molecular vibrations. Figure 2b shows the spectrum measured following a 2-h deposition of $(O_2N)_2C-(CH_2)_2N^{15}NO_2$. Note that a band at 1552.6 $cm^{-1}$ (39) is present with two side bands at 1554.6 and 1550.4 $cm^{-1}$, similar to band 39 in the natural abundance TNAZ spectrum. Bands 41 and 40 are again observed along with a band consistent with one at 1589.2 $cm^{-1}$, indicating that some natural abundance TNAZ is present. Most other bands above 1200 $cm^{-1}$ have absorptions very near those of the dominant isotope of natural abundance TNAZ, with the exception of an absorption at 1313.0 $cm^{-1}$ (34) that is shifted 11.5 $cm^{-1}$. The same spectrum from 1250 to 600 $cm^{-1}$ is shown in Figure 3b. Again most absorptions for $(O_2N)_2C(CH_2)_2N^{15}NO_2$ are very close to those of the dominant isotope of natural abundance TNAZ with the exceptions of bands at 903.9, 811.1, and 750.5 $cm^{-1}$ (23, 20, and 19), which are respectively 0.3, 6.1, and 15.7 $cm^{-1}$ from their corresponding natural abundance TNAZ absorptions.

Figure 2c shows the spectrum measured following a 2-h deposition of $(O_2{}^{15}N)_2-C(CH_2)_2N-{}^{15}NO_2$. Close inspection

**TABLE 3: Calculated and Observed Fundamental Frequencies ($cm^{-1}$) and IR Intensities of 1,3,3-Trinitroazetidine**

| mode no. | mode sym. | observed | HF 6-31G** | HF (0.89) 6-31G** | IR intensity | MP2 6-31G** | IR intensity | BP86 6-31G** | IR intensity | B3P86 6-31G** | IR intensity | B3LYP 6-31G** | IR intensity |
|---|---|---|---|---|---|---|---|---|---|---|---|---|---|
| 12 | A′ | | 472.6 | 420.6 | 2.4 | 428.6 | 1.2 | 391.1 | 0.1 | 422.2 | 0.5 | 416.0 | 0.4 |
| 13 | A″ | | 577.3 | 513.8 | 12.1 | 530.2 | 2.7 | 501.4 | 4.0 | 527.6 | 5.2 | 521.9 | 5.4 |
| 14 | A′ | | 625.4 | 556.6 | 47.3 | 560.4 | 14.9 | 510.0 | 6.3 | 558.1 | 15.0 | 545.1 | 14.0 |
| 15 | A″ | | 675.8 | 601.4 | 3.2 | 609.8 | 0.4 | 586.9 | 1.1 | 620.7 | 1.3 | 610.2 | 1.4 |
| 16 | A′ | 658.5 | 770.4 | 685.6 | 55.2 | 681.8 | 16.8 | 623.5 | 6.8 | 676.5 | 15.3 | 664.4 | 14.3 |
| 17 | A′ | 712.3 | 817.6 | 727.6 | 5.9 | 708.9 | 5.4 | 685.0 | 1.2 | 730.7 | 1.4 | 719.7 | 1.9 |
| 18 | A″ | | 823.9 | 733.2 | 0.6 | 712.9 | 0.6 | 689.3 | 1.1 | 731.9 | 1.8 | 722.4 | 1.6 |
| 19 | A′ | 766.2 | 891.3 | 793.3 | 39.7 | 764.3 | 26.9 | 734.0 | 19.1 | 784.7 | 25.1 | 772.1 | 24.9 |
| 20 | A′ | 817.2 | 931.4 | 829.0 | 4.6 | 820.3 | 5.3 | 788.0 | 4.9 | 831.8 | 1.3 | 822.7 | 2.9 |
| 21 | A′ | 840.9 | 962.7 | 856.8 | 42.5 | 839.9 | 49.9 | 813.3 | 48.7 | 863.8 | 44.9 | 850.9 | 45.5 |
| 22 | A′ | 864.8 | 1009.7 | 898.6 | 10.8 | 886.6 | 15.7 | 820.5 | 55.1 | 883.1 | 43.2 | 869.5 | 42.7 |
| 23 | A′ | | 1027.3 | 914.3 | 18.4 | 938.4 | 19.8 | 876.9 | 19.9 | 932.5 | 17.6 | 918.1 | 16.4 |
| 24 | A″ | 905.8 | 1059.2 | 942.7 | 0.1 | 966.2 | 0.7 | 906.4 | 0.5 | 944.7 | 0.3 | 949.8 | 0.4 |
| 25 | A′ | 1035.3 | 1227.8 | 1092.7 | 21.0 | 1087.9 | 49.1 | 999.7 | 63.5 | 1086.0 | 38.6 | 1062.3 | 49.0 |
| 26 | A″ | 1091.1 | 1231.4 | 1095.9 | 5.1 | 1140.9 | 6.4 | 1067.8 | 3.7 | 1125.6 | 2.1 | 1109.6 | 4.7 |
| 27 | A″ | | 1251.5 | 1113.9 | 1.7 | 1152.1 | 0.2 | 1086.3 | 0.5 | 1134.3 | 1.5 | 1130.7 | 0.0 |
| 28 | A′ | 1123.0 | 1274.2 | 1134.0 | 3.1 | 1175.7 | 13.8 | 1096.0 | 12.5 | 1150.9 | 13.1 | 1146.0 | 6.5 |
| 29 | A′ | 1158.7 | 1344.0 | 1208.1 | 48.4 | 1207.0 | 35.2 | 1116.7 | 35.0 | 1204.9 | 17.8 | 1183.0 | 45.5 |
| 30 | A″ | 1207.3 | 1357.4 | 1196.2 | 4.6 | 1207.0 | 10.9 | 1143.8 | 7.0 | 1217.0 | 9.4 | 1193.4 | 6.8 |
| 31 | A′ | 1215.3 | 1386.3 | 1233.8 | 65.2 | 1258.8 | 54.5 | 1163.1 | 57.1 | 1240.1 | 73.7 | 1227.9 | 62.3 |
| 32 | A″ | | 1430.4 | 1273.0 | 1.0 | 1292.6 | 0.5 | 1217.1 | 0.9 | 1273.3 | 0.5 | 1277.3 | 0.9 |
| 33 | A′ | 1276.7 | 1488.2 | 1324.5 | 61.4 | 1334.1 | 90.2 | 1241.3 | 71.4 | 1312.6 | 46.4 | 1306.3 | 88.6 |
| 34 | A′ | 1324.5 | 1603.2 | 1426.9 | 511.7 | 1351.4 | 71.6 | 1300.4 | 225.5 | 1406.1 | 370.6 | 1375.6 | 309.3 |
| 35 | A′ | 1329.5 | 1639.9 | 1459.5 | 20.0 | 1383.1 | 76.8 | 1308.2 | 145.0 | 1413.2 | 130.4 | 1382.3 | 111.8 |
| 36 | A′ | 1362.8 | 1643.8 | 1463.0 | 140.7 | 1390.2 | 202.6 | 1353.9 | 99.1 | 1457.0 | 73.6 | 1426.8 | 74.5 |
| 37 | A″ | 1441.5 | 1658.8 | 1476.4 | 27.9 | 1528.6 | 12.2 | 1437.7 | 23.7 | 1484.3 | 23.4 | 1493.4 | 21.7 |
| 38 | A′ | 1458.7 | 1680.1 | 1495.3 | 27.9 | 1548.9 | 8.1 | 1456.4 | 7.3 | 1507.3 | 5.1 | 1513.1 | 7.3 |
| 39 | A″ | 1589.2 | 1862.6 | 1657.7 | 510.4 | 1825.7 | 146.1 | 1608.5 | 204.8 | 1725.5 | 277.3 | 1681.5 | 268.3 |
| 40 | A″ | 1585.6 | 1893.0 | 1684.8 | 519.5 | 1832.4 | 12.2 | 1616.4 | 170.8 | 1734.4 | 199.8 | 1689.6 | 192.3 |
| 41 | A′ | 1593.2 | 1898.3 | 1689.5 | 546.4 | 1833.9 | 46.0 | 1619.0 | 175.4 | 1737.2 | 227.3 | 1692.2 | 217.6 |
| 42 | A″ | | 3307.4 | 2943.5 | 0.1 | 3166.2 | 0.1 | 3017.7 | 1.2 | 3112.9 | 0.1 | 3105.7 | 0.4 |
| 43 | A′ | 2907.4 | 3311.7 | 2947.4 | 2.2 | 3169.7 | 3.0 | 3022.7 | 3.6 | 3117.9 | 3.9 | 3110.6 | 3.6 |
| 44 | A′ | 2979.4 | 3394.0 | 3020.7 | 0.6 | 3264.6 | 0.4 | 3093.7 | 0.1 | 3193.6 | 0.6 | 3181.2 | 0.7 |
| 45 | A″ | 3023.3 | 3392.2 | 3019.0 | 0.3 | 3264.8 | 0.6 | 3093.9 | 1.0 | 3193.8 | 0.9 | 3181.4 | 0.3 |

of the $NO_2$ region reveals bands at 1558.9 (41) and 1551.3 (40) $cm^{-1}$ and one at 1552.7 $cm^{-1}$ (39), which also has a site splitting band at 1553.9 $cm^{-1}$. As expected, all three are shifted substantially from their corresponding natural abundance TNAZ absorptions. Absorptions corresponding to bands 37−33 are present and listed in Table 1; all of these absorptions are significantly shifted relative to natural abundance TNAZ. Bands 36 and 34 shifted the most, 21.4 and 19.6 $cm^{-1}$, respectively. Similarly in the lower energy region shown in Figure 3c, several absorptions are shifted, the largest being at 749.7 $cm^{-1}$ (19) shifted 16.5 $cm^{-1}$ from natural abundance TNAZ.

The spectrum for $(O_2N)_2-{}^{13}C(CH_2)_2N-NO_2$ shown in Figure 2d reveals an unexpected shift in the 1600−1500 $cm^{-1}$ region. Although the substitution of a heavier isotope should shift molecular vibrations to the red, the band at 1593.4 $cm^{-1}$ (40) is observed 5.7 $cm^{-1}$ to the blue of its analogous natural abundance absorption frequency. Absorptions for all other bands above 1200 $cm^{-1}$ are very near those of the natural abundance material. In contrast, Figure 3d illustrates that several bands below 1200 $cm^{-1}$ shifted appreciably, the largest being a band at 1069.9 $cm^{-1}$ (26), which is red shifted 26.2 $cm^{-1}$.

**Quantum Chemical Calculations.** Geometry optimizations all converged on a $C_s$ structure (Figure 1). Calculated geometries are listed in Table 2 for all five computational methods. In addition, X-ray crystallographic data published by Archibald et al. are provided.[5] Crystal lattice effects result in a $C_1$ structure as indicated by the unequal C−C bond distances of 1.534 and 1.545 Å.[5]

Computed frequencies for modes above 400 $cm^{-1}$ are tabulated in Table 3. Again, calculations at five levels of theory are provided along with calculated intensities. Scaled (0.89) Hartree−Fock values are also included. Calculated synthetic spectra are presented in Figures 4a−e and 5a−e. Mode number assignments are as calculated by BP86. Very weak transitions are not labeled.

Calculations for isotopically labeled species provide additional comparisons to experimental data, as well as simplified analyses of a specific atom's participation in fundamental vibrations. Figure 6 shows DFT-calculated spectra for TNAZ and isotopically labeled TNAZ using BP86/6-31G**. Note that calculated distinctions between $N-NO_2$ and $C-NO_2$ antisymmetric stretches are apparent in bands 41, 40, and 39 in the $^{15}NO_2$-labeled samples of Figure 6 (a, c, and d). Bands below 1600 $cm^{-1}$ are not simple localized vibrations; all have significant mode mixing, particularly with $CH_2$ bends and ring modes. The vibrations that involve appreciable N−N and N−CN stretching modes are in the 1400−1200 $cm^{-1}$ region marked 36, 35, and 34. Finally, the bands marked 33−25 have significant ring motion in their assignments.

Comparing the calculated and observed shift of a particular vibration upon isotopic substitution also provides a means of comparing different quantum chemical methods. Since the varying degree of mode mixing calculated using various levels of theory results in more or less participation of specific atoms, such comparisons provide a qualitative evaluation of which methods best describe specific modes. Calculated isotopic shifts for all five methods are listed in Table 4. Comparisons among various methods of calculation will be provided in the discussion section that follows.

## Discussion

**Experimental Spectra.** Spectra of natural abundance and isotopically labeled TNAZ permit assignment of experimental

**TABLE 4: Calculated and Observed Isotopic Shifts of Selected Fundamental Vibrations for TNAZ**

| mode no. | mode sym. | obsvd $\delta$ | HF(0.89) calcd | MP2 calcd | BP86 calcd | B3P86 calcd | B3LYP calcd |
|---|---|---|---|---|---|---|---|
| | | (a) $(O_2N)_2-C(CH_2)_2N-{}^{15}NO_2$ | | | | | |
| 41 | A′ | −0.3 | 0.0 | 0.0 | 0.0 | 0.0 | 0.0 |
| 40 | A″ | −0.3 | 0.0 | 0.0 | 7.7 | 0.0 | 0.0 |
| 39 | A″ | 36.6 | 43.3 | 41.2 | 29.5 | 39.8 | 38.9 |
| 34 | A′ | 11.5 | 26.1 | 13.7 | 9.1 | 20.4 | 16.9 |
| 23 | A′ | 0.3 | 2.7 | 1.5 | 2.3 | 2.7 | 2.3 |
| 20 | A′ | 6.1 | 10.4 | 6.4 | 6.2 | 6.6 | 6.4 |
| 19 | A′ | 15.7 | 15.9 | 16.3 | 17.0 | 17.4 | 17.5 |
| | | (b) $(O_2{}^{15}N)_2-C(CH_2)_2N-{}^{15}NO_2$ | | | | | |
| 41 | A′ | 34.3 | 42.9 | 40.6 | 36.1 | 38.8 | 37.8 |
| 40 | A″ | 34.3 | 42.5 | 40.4 | 37.3 | 38.8 | 37.8 |
| 39 | A″ | 36.5 | 43.3 | 41.4 | 35.9 | 39.8 | 38.9 |
| 38 | A′ | 0.8 | 22.0 | 0.4 | 1.0 | 1.8 | 1.0 |
| 37 | A″ | 0.0 | 8.0 | 0.0 | 0.1 | 0.0 | 0.1 |
| 36 | A′ | 21.4 | 14.6 | 16.2 | 19.1 | 22.1 | 21.5 |
| 35 | A′ | 12.4 | 12.4 | 19.2 | 16.2 | 20.4 | 19.1 |
| 34 | A′ | 19.6 | 26.1 | 23.5 | 17.6 | 20.9 | 19.1 |
| 33 | A′ | 8.5 | 1.6 | 10.7 | 4.3 | 2.5 | 4.8 |
| 22 | A′ | 4.2 | 7.9 | 6.5 | 8.9 | 8.6 | 8.6 |
| 21 | A′ | 7.8 | 10.0 | 8.1 | 8.3 | 8.8 | 8.6 |
| 20 | A′ | 7.5 | 11.2 | 8.8 | 7.3 | 7.9 | 7.5 |
| 19 | A′ | 16.5 | 17.6 | 17.4 | 17.4 | 18.1 | 18.1 |
| | | (c) $(O_2N)_2-{}^{13}C(CH_2)_2N-NO_2$ | | | | | |
| 37 | A″ | 0.9 | 1.3 | 0.0 | 0.0 | 0.0 | 0.0 |
| 33 | A′ | 2.9 | 2.9 | 5.3 | 3.5 | 0.1 | 0.9 |
| 31 | A′ | 23.3 | 17.8 | 14.5 | 9.8 | 12.8 | 12.5 |
| 30 | A″ | 4.9 | 3.9 | 6.5 | 4.0 | 2.9 | 4.1 |
| 29 | A′ | 12.2 | 13.1 | 15.6 | 13.2 | 13.5 | 12.9 |
| 28 | A′ | 6.8 | 7.3 | 7.5 | 10.6 | 9.8 | 10.2 |
| 26 | A″ | 21.2 | 27.0 | 22.6 | 22.0 | 23.4 | 25.8 |
| 22 | A′ | 4.2 | 2.0 | 3.1 | 1.6 | 1.8 | 2.0 |
| 21 | A′ | 7.8 | 1.0 | 0.3 | 0.6 | 0.6 | 0.6 |

frequencies. Mode mixing is expected for many bands of TNAZ. Bands at 3027.3, 2979.4, and 2907.4 $cm^{-1}$ (45−43) are weak but track with all other bands. Isotopic shifts are not observed. The bands that appear in the region expected for $CH_2$ stretching modes are in agreement with quantum mechanical calculations and are accordingly assigned to $CH_2$ antisymmetric and symmetric stretches.

Each of the three nitro groups of TNAZ is unique because of the differing orientations of the *gem*-dinitro groups. If resolved, three distinct bands corresponding to antisymmetric $NO_2$ stretches are expected in the 1600 $cm^{-1}$ region. The 36.6 $cm^{-1}$ shift of band 39 in $(O_2N)_2-C(CH_2)_2N-{}^{15}NO_2$ samples is sufficient to assign band 39 to the antisymmetric stretch of the nitramine $RN-NO_2$ group. Similarly in $(O_2{}^{15}N)_2-C(CH_2)_2-N-{}^{15}NO_2$ samples, bands 41 and 40 ($C-(NO_2)_2$) both shifted by 34.3 $cm^{-1}$ and are assigned to the antisymmetric stretches of the two *gem*-dinitro groups. The blue shift of band 40 in $(O_2N)_2{}^{13}C(CH_2)_2NNO_2$ is attributed to interaction with a combination or overtone of band(s) below 575 $cm^{-1}$.

Bands 38 and 37 at 1458.7 and 1441.5 $cm^{-1}$ appear in the region expected for $CH_2$ bends. Isotopically labeled spectra show little coupling to the central carbon atoms or nitrogen atoms of the $NO_2$ groups. This effect is in agreement with quantum chemical calculations, and the bands are accordingly assigned to $CH_2$ bending modes. Calculations predict bands below 1400 $cm^{-1}$ to be nonlocal modes. In fact bands 36, 35, and 34 all involve participation of the nitrogen atoms of the *gem*-dinitro groups, as indicated by the relatively large isotopic shifts of 21.4, 12.4, and 19.6 $cm^{-1}$ in $(O_2{}^{15}N)_2-C(CH_2)_2N-{}^{15}NO_2$ samples. In addition, involvement of the $N-NO_2$ group is apparent for band 34 from its isotopic shift of 11.5 $cm^{-1}$ in $(O_2N)_2-C(CH_2)_2N-{}^{15}NO_2$ samples. The ring carbon atoms are not involved in these vibrations but quantum chemical calculations predict $CH_2$ bending participation in bands 36 and 35, while band 34 is calculated to have $NO_2$ bending contributions.

Bands 33−24 involve ring motions, as indicated by relatively large isotopic shifts with $(O_2N)_2-{}^{13}C(CH_2)_2N-NO_2$ samples. Calculations also predict all of these modes to have significant coupling with $CH_2$ and $NO_2$ motions. The degree of involvement of specific subunits of the molecule in these vibrations can be determined from experimental spectra of available isotopically labeled TNAZ. On the basis of the results presented here, vibrations corresponding to modes 31−28, 26, 25, 22, 21, and 16 all involve the ring carbon bearing the *gem*-dinitro groups.

**Quantum Chemical Calculations.** Direct comparisons of calculated and observed geometries are complicated because the calculations are on an individual TNAZ molecule, while X-ray data were collected for crystalline TNAZ. Trends among calculations are of interest. Overall, all of the computed geometries are in good agreement with the X-ray experimental data, although certain bond lengths and one bond angle are poorly predicted. Only the HF method gives an accurate N−N distance; all correlated approaches considerably overestimate the bond length, the worst for this bond being BP86. On the other hand, the HF N−O bond lengths are significantly underestimated. The correlated methods, particularly the MP2 and BP86, give low values for the N−N−C angles.

Lattice effects produce differences between the N(5)−O bonds, the N(1)−C bonds, and the C(3)−C bonds. The N(6)−O bonds are unique because they are the only nonequivalent N−O bonds in the $C_s$ point group. Note in Figure 1 that possible interactions between hydrogen atoms of the ring and O(6b) could result in different N(6)−O bond lengths. The X-ray structure indicates that the N(6)−O(6b) bond is about 0.01 Å longer than the N(6)−O(6a). Although HF underestimates both bond lengths by about 0.03 Å, the nonequivalence of the bonds is reproduced. In contrast, MP2 predicts bond distances that are effectively the same. The DFT methods predict N(6)−O(6b) to be longer by ∼0.005 Å.

Table 3 lists calculated and observed frequencies for all assigned transitions of TNAZ. Bands 45−43 correspond to $CH_2$ stretching frequencies. Scaled HF calculations estimate the three bands to within 41 $cm^{-1}$. BP86 calculates these modes to within 120 $cm^{-1}$, whereas B3P86, B3LYP, MP2, and unscaled HF all overestimate them by >200 $cm^{-1}$. Comparisons between calculated and observed spectra are presented in Figures 4 and 5. The HF results are scaled by 0.89. The calculated antisymmetric $NO_2$ stretches of bands 41, 40, and 39 are best described by BP86, which predicts the frequencies within 30 $cm^{-1}$ whereas the next best, scaled HF, is off by more than 100 $cm^{-1}$, particularly miscalculating bands 41 and 40 corresponding to the *gem*-dinitro groups. B3LYP and B3P86 both calculate the bands to within 150 $cm^{-1}$. MP2 is off by about 240 $cm^{-1}$.

Bands 38 and 37 correspond to predominantly $CH_2$ bends. Comparing computational methods gives an order of accuracy of BP86 > scaled HF > B3P86 > B3LYP > MP2 > unscaled HF. The BP86 method has calculated both of these modes within 5 $cm^{-1}$ of their observed values.

Bands 36−34 are primarily attributed to N−N and N−CN stretches. The accuracy of computational descriptions of these vibrations is of particular interest since it is believed that loss of $NO_2$ is a likely initial step in the combustion of TNAZ.[9,10,12] The BP86 method is the most accurate, underestimating each of the modes by ∼25 $cm^{-1}$, whereas B3LYP and B3P86 overestimate them by roughly 60 and 100 $cm^{-1}$, respectively. In addition, the mode descriptions provided by all three DFT methods appear to be markedly different from those provided

by HF and MP2. Note that a single band, marked 34, is calculated by HF to be much more intense than others in the 1500−1300 $cm^{-1}$ region in Figure 4a. In contrast, MP2, shown in Figure 4b, predicts all three bands to be strong with the most intense band (36) calculated to be the highest in frequency. On the other hand, BP86, B3P86, and B3LYP all predict relative band intensities of bands 36, 35, and 34 in reasonable agreement with the experimental spectrum.

Several of the bands below 1300 $cm^{-1}$ (listed in Table 1) are calculated to involve predominantly ring modes coupled with $CH_2$ modes. Band 33 is the highest frequency ring mode and one of the more intense ring vibrations in Figure 4f. Interestingly, again BP86 underestimates the transition by 35 $cm^{-1}$, while B3P86 and B3LYP overestimate by 35 and 30 $cm^{-1}$, respectively. Scaled HF and MP2 similarly overestimate this band by 50 and 60 $cm^{-1}$, respectively. Trends for ring modes 31−25 mirror those described for band 33. In each case, B3LYP predicts the frequency within 30 $cm^{-1}$, while B3P86 overestimates it by about 50 $cm^{-1}$. BP86 systematically underestimates the modes by 40−50 $cm^{-1}$.

The descriptions of vibrational modes can also be qualitatively studied by comparing calculated and observed differences for fundamental vibrations of natural abundance and isotopically labeled TNAZ, shown in Table 4. Unfortunately this technique is complicated by interactions not accounted for in standard quantum chemical calculations that may arise between combination and overtones of low-lying vibrations. For instance, none of the calculations here predicted band 40 of $(O_2N)-{}^{13}C(CH_2)_2-N-NO_2$ to be blue shifted from the natural abundance fundamental.

In spite of such interactions, interesting differences are apparent between the isotopic calculations presented in Table 4. For instance, although BP86 most closely calculates the $NO_2$ antisymmetric stretching frequencies (41, 40, 39), it also predicts coupling between the nitramine and *gem*-dinitro groups as indicated by the calculated shift of 7.7 $cm^{-1}$ for band 40 upon $^{15}N$ substitution of the nitramine nitro group (Table 4a). The coupling is not observed, and the $\delta$ value for mode 39 appears to be slightly better described by either B3P86 or B3LYP. In spite of this, BP86 better estimates the participation of the $^{15}N$ atom than both B3P86 and B3LYP for all other modes. Similarly for the $(O_2{}^{15}N)_2-C(CH_2)_2N-{}^{15}NO_2$ samples, BP86 better calculates the involvement of the N atoms of all three nitro groups.

In contrast to calculated and observed $\delta$'s for $^{15}N$-labeled samples, interesting distinctions arise when examining the $(O_2N)_2-{}^{13}C(CH_2)_2N-NO_2$ data. For bands 33, 31, and 28, all ring modes, both HF and MP2 provide competitive results. These methods more closely calculate the involvement of the carbon atom C(3). This may suggest a possible problem with DFT methods for calculating some of the ring fundamental vibrations in strained systems. Again, the extents of such problems are difficult to quantify, due to possible uncalculated interactions between fundamental vibrations.

## Conclusions

We have obtained a well-resolved, matrix-isolated TNAZ spectrum and used it to carry out a detailed assessment of several quantum chemical calculations. Comparisons of calculated and observed spectra shown in Figures 4 and 5 and Table 3 indicate that density functional theory, which is computationally less expensive, is generally more accurate than second-order Moller−Plesset theory. Overall the best results were obtained with the BP86 and B3LYP methods and the scaled HF results. The poorest overall predictions are given by MP2. These conclusions generally agree with the results of an extensive study of computed vibrational frequencies for 122 molecules.[15]

**Acknowledgment.** We thank T. Hismith and R. Wordle of Thiokol Inc. for providing raw TNAZ samples and J. Oxley, M. Hiskey, and M. Coburn for providing the isotopically labeled samples. C.A.T., J.K.R., and T.P.R. acknowledge the Office of Naval Research and the Naval Research Laboratory, for financial support provided as part of the Accelerated Research Initiative on the Heterogenous Decomposition of Energetic Materials, and the Department of Defense High Performance Computing facility at Army CEWES, MS, for a computing time grant. T.P.R., J.M.S., and P.P. appreciate the financial support of the Office of Naval Research by the Program Officer Richard S. Miller.

## References and Notes

(1) Aubert, S. A. WL-TR-94-7049; Wright Laboratory, Armament Directorate, Munitions Division, Energetic Materials Branch, August, 1994.
(2) Iyer, S.; Velicky, R.; Sandus, O.; Alster, J. Technical Report ARAED-TR-89010, June 1989.
(3) Oyumi, O.; Brill, T. B. *Combust. Flame* **1985**, *62*, 225.
(4) Oehrle, S. A. *J. Energ. Mater.* **1996**, *14*, 47.
(5) Archibald, T. G.; Gilardi, R.; Baum, K.; George, C. *J. Org. Chem.* **1990**, *55*, 2920.
(6) Archibald, T. G.; Garver, L. C.; Malik, A. A.; Bonsu, F. O.; Tzeng, D. D.; Preston, S. B.; Baum, K. Research in Energetic Compounds. Contract 200014-78-C-0147; Fluorochem, inc.: Azusa, CA.; ONR-2-10, Feb 1988; 78 p.
(7) McKenney, R. L., Jr.; Floyd, T. G.; Stevens, W. E.; Marchand, A. P.; Sharma, G. V. M.; Bott, S. G.; Archibald, T. G. WL-TR-96-7046; Wright Laboratory, Armament Directorate July 1996.
(8) Oyumi, Y.; Brill, T. B.; Rheingold, A. L.; Haller, T. M. *J. Phys. Chem.* **1985**, *89*, 4317.
(9) Anex, D. S.; Allman, J. C.; Lee, Y. T. In *Chemistry of Energetic Materials*; Olah, G., Squire, D. R., Eds.; Academic Press: New York, 1991; Chapter 2, pp 27−54.
(10) Bulusu, S.; Behrens, R., Jr. *Def. Sci. J.* **1996**, *46*, 347.
(11) Oxley, J.; Smith, J.; Zheng, W.; Rogers, E.; Coburn, M. *J. Phys. Chem. A* **1997**, *101*, 4375.
(12) Politzer, P.; Seminario, J. *Chem. Phys. Lett.* **1993**, *207*, 27.
(13) Pai, S. V.; Chabalowski, C. F.; Rice, B. M. *J. Phys. Chem.* **1996**, *100*, 15368.
(14) Wong, M. W. *Chem. Phys. Lett.* **1996**, *256*, 391.
(15) Scott, A. P.; Radom, L. *J. Phys. Chem.* **1996**, *100*, 16502.
(16) El-Azhary, A. A.; Suter, H. U. *J. Phys. Chem.* **1996**, *100*, 15056.
(17) Martin, J. M. L.; El-Yazal, J.; Francois, J. *J. Phys. Chem.* **1996**, *100*, 15358.
(18) Coburn, M.; Hiskey, M.; Oxley, J.; Smith, J.; Zheng, W.; Rogers, E. *J. Energ. Mater.*, accepted for publication.
(19) Frisch, M. J.; Trucks, G. W.; Schlegel, H. B.; Gill, P. M. W.; Johnson, B. G.; Robb, M. A.; Cheeseman, J. R.; Keith, T.; Petersson, G. A.; Montgomery, J. A.; Raghavachari, K.; Al-Laham, M. A.; Zakrzewski, V. G.; Ortiz, J. V.; Foresman, J. B.; Cioslowski, J.; Stefanov, B. B.; Nanayakkara, A.; Challacombe, M.; Peng, C. Y.; Ayala, P. Y.; Chen, W.; Wong, M. W.; Andres, J. L.; Replogle, E. S.; Gomperts, R.; Martin, R. L.; Fox, D. J.; Binkley, J. S.; Defrees, D. J.; Baker, J.; Stewart, J. P.; Head-Gordon, M.; Gonzalez, C.; Pople, J. A. *Gaussian 94, Revision D.1*; Gaussian, Inc.: Pittsburgh PA, 1995.
(20) Becke, A. D. *J. Chem. Phys.* **1993**, *98*, 5648.
(21) Perdew, J. P.; Wang, Y. *Phys. Rev. B.* **1992**, *45*, 13244.
(22) Perdew, J. P. *Phys. Rev. B.* **1986**, *33*, 8822.
(23) Becke, A. D. *Phys. Rev. A.* **1988**, *38*, 3098.
(24) Lee, C.; Yang, W.; Parr, R. G. *Phys. Rev. B* **1988**, *37*, 785.